

## CHAPTER 4

### RESULTS AND DISCUSSION



#### 4.1 Parametric study

From Chapter 3, the balance equation for NAPL-water-soil system and constitutive equations for NAPL-water relationship have been implemented in the computer code U\_DYSAC2. The modified computer code has been used to simulate the NAPL transport patterns. In this section, NAPL transport case studies have been simulated to explain the effects of physical properties of NAPL by considering its density and viscosity and the effect of water flow in porous media.

##### 4.1.1 DNAPL movement in static saturated porous media.

This simulation case is defined in Figure 4.1; a two-dimensional soil box (0.3 m. x 0.5 m.) is simulated. To control flow in system, this problem is assumed to have impermeable layers at the bottom, the sides, and the top of the box, except at the DNAPL source. The DNAPL source is controlled by the pressure head of DNAPL. The boundary conditions are defined as follows:

- DNAPL source :  $P_w = 0, P_N = 0.5 \text{ kPa}$
- Top :  $Q_w = Q_N = 0 \text{ cm}^3/\text{sec}$
- Lateral sides :  $Q_w = Q_N = 0 \text{ cm}^3/\text{sec}$
- Bottom :  $Q_w = Q_N = 0 \text{ cm}^3/\text{sec}$

where  $P_\alpha$  ( $\alpha = W, N$ ) represents the pressure of fluid ( water and DNAPL) in excess of atmospheric pressure.  $Q_\alpha$  is the fluid flux in the direction normal to the boundary.

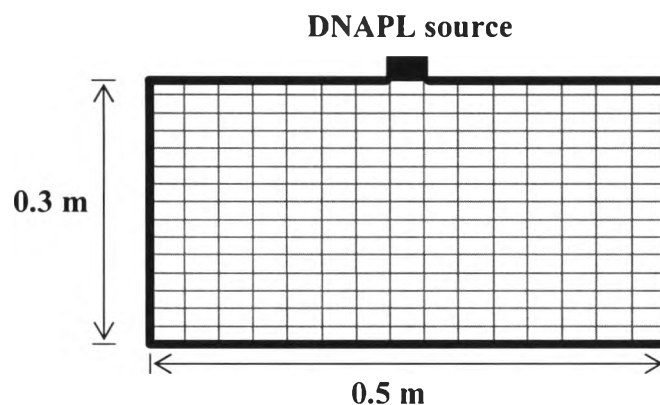


**Figure 4.1:** Solution domain for DNAPL movement in static saturated porous media (all dimensions are in meters)

At  $t = 0$ , the soil box is fully saturated with water and the water pressure is hydrostatic. Then the DNAPL is released from source with constant head (0.5 kPa).

For numerical simulation, the soil box is divided into 255 elements (15 elements x 15 elements). The soil and DNAPL parameters are shown in Table 4.1.

Results from the simulation are shown in Figure 4.2 as contours of water saturation. At a time of 10 seconds, DNAPL just starts to move into the soil box with the influence of DNAPL source pressure. The plume shows a semi-circle shape as shown in Figure 4.2.A, because at the beginning the source pressure is driving the flow. After that, as shown in Figure 4.2.B, the density of DNAPL plays a role in the DNAPL movement. The plume shape changes from a semi-circle to be more oval like due to the density of the DNAPL.

After about 100 seconds, the DNAPL reaches the bottom and begins to settle at the bottom. The DNAPL then accumulates at the bottom and spreads horizontally, as shown in Figures 4.2 D.

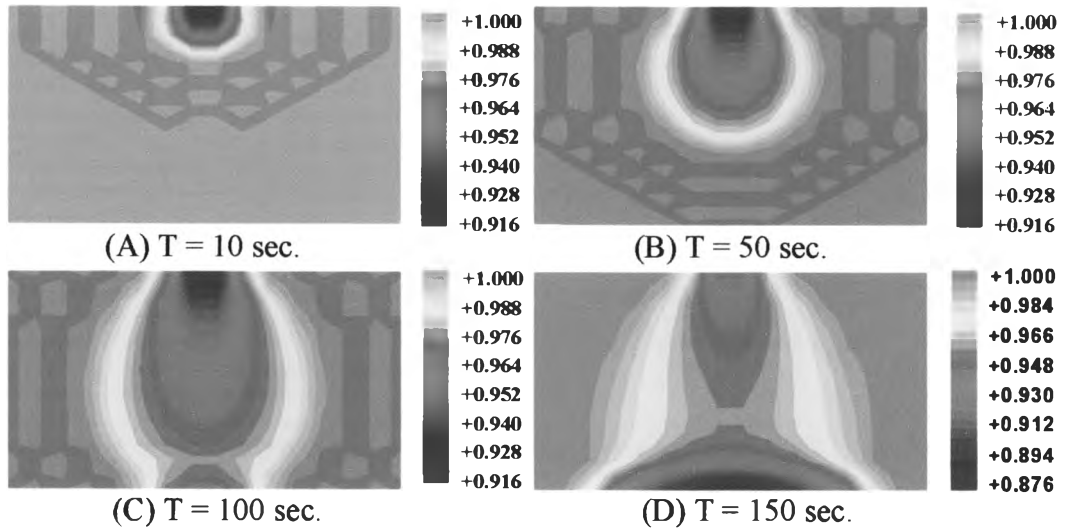


**Figure 4.2:** Water saturation contour: DNAPL movement in a static saturated porous media.

**Table 4.1:** Material parameter of static saturated porous media case.

Material parameters	Symbols	Values
Soil grain density	$\rho_s$	$2.7 \times 10^3 \text{ kg/m}^3$
Water density	$\rho_w$	$1.0 \times 10^3 \text{ kg/m}^3$
DNAPL density	$\rho_N$	$1.63 \times 10^3 \text{ kg/m}^3$
Bulk modulus of water	$K_w$	$0.43 \times 10^{10} \text{ kPa}$
Bulk modulus of DNAPL	$K_N$	$1.0 \times 10^6 \text{ kPa}$
Water viscosity	$\mu_w$	$1.0 \times 10^{-3} \text{ Pa.s}$
DNAPL viscosity	$\mu_N$	$2.3 \times 10^{-3} \text{ Pa.s}$
Intrinsic permeability	$K$	$5.0 \times 10^{-10} \text{ m}^2$
Irreversible water saturation of soil	$S_{irr}$	0.2
Van Genuchten parameter	$\lambda$	$0.11 \text{ cm}^{-1}$
	$N$	1.84
Soil porosity	$N$	0.4
Initial water saturation	$S_{int}$	1.0

#### 4.1.2 Effects of DNAPL density and viscosity on DNAPL movement.

In order to study the influence of DNAPL density and viscosity on its movement, eight numerical simulations are carried out using the same model as shown in Fig. 4.2. The source boundary is assigned DNAPL pressure ( $P_N$ ) = 0.5 kPa and water pressure ( $P_w$ ) = 0.0 kPa. The porous media properties used are listed in Table 4.1. Table 4.2 lists DNAPL properties assigned for various cases. The density of NAPL is varied from  $1.0 \times 10^3$  to  $2.0 \times 10^3$  kg/m<sup>3</sup> and the viscosity is varied from  $0.7 \times 10^{-3}$  to  $5 \times 10^{-3}$  Pa.s. Discussions are based on visual observation of the simulated results.

**Table 4.2:** Fluid properties assigned for studying the effects of fluid density and viscosity.

	$\rho_w$ (kg/m <sup>3</sup> )	$\rho_N$ (kg/m <sup>3</sup> )	$\mu_w$ (Pa.s)	$\mu_N$ (Pa.s)
Vary density				
Base case	$1.00 \times 10^3$	$1.63 \times 10^3$	$1.00 \times 10^{-3}$	$2.30 \times 10^{-3}$
Run 1	$1.00 \times 10^3$	$1.00 \times 10^3$	$1.00 \times 10^{-3}$	$2.30 \times 10^{-3}$
Run 2	$1.00 \times 10^3$	$1.30 \times 10^3$	$1.00 \times 10^{-3}$	$2.30 \times 10^{-3}$
Run 3	$1.00 \times 10^3$	$2.00 \times 10^3$	$1.00 \times 10^{-3}$	$2.30 \times 10^{-3}$
Vary viscosity				
Base case	$1.00 \times 10^3$	$1.63 \times 10^3$	$1.00 \times 10^{-3}$	$2.30 \times 10^{-3}$
Run 4	$1.00 \times 10^3$	$1.63 \times 10^3$	$1.00 \times 10^{-3}$	$0.70 \times 10^{-3}$
Run 5	$1.00 \times 10^3$	$1.63 \times 10^3$	$1.00 \times 10^{-3}$	$1.00 \times 10^{-3}$
Run 6	$1.00 \times 10^3$	$1.63 \times 10^3$	$1.00 \times 10^{-3}$	$1.50 \times 10^{-3}$
Run 7	$1.00 \times 10^3$	$1.63 \times 10^3$	$1.00 \times 10^{-3}$	$5.00 \times 10^{-3}$

The base case simulation, as shown in Figure 4.2, shows a moderate degree of pooling and flow of DNAPL. The results from the increased density case (Figure 4.2 D) shows that the vertical rate of DNAPL plume movement increases due to the greater gravity driving force. For Figure 4.3.A, when the density of DNAPL decreases to nearly the density of water, the gravity driving force has no effect. The plume spreads by the influence of DNAPL source pressure in a semi-circular shape, and the plume stops spreading when the pressure of the DNAPL source is in equilibrium with the pressure of water in the soil.

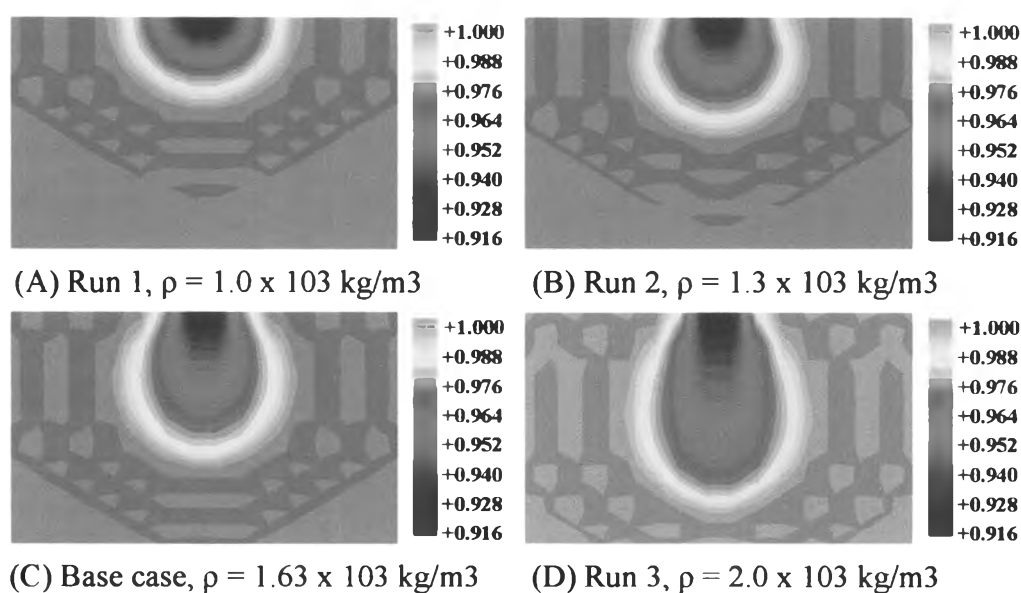


**Figure 4.3:** Water saturation contours showing the distribution of DNAPL at  $t= 50$

seconds for various DNAPL densities

- (A) Run 1:  $\rho_N = \rho_w = 1.0 \times 10^3 \text{ kg/m}^3$
- (B) Run 2: the density of DNAPL is decreased to  $\rho_N = 1.3 \times 10^3 \text{ kg/m}^3$
- (C) Base case simulation:  $\rho_N = 1.63 \times 10^3 \text{ kg/m}^3$
- (D) Run 3: the density of DNAPL is increased to  $\rho_N = 2.0 \times 10^3 \text{ kg/m}^3$

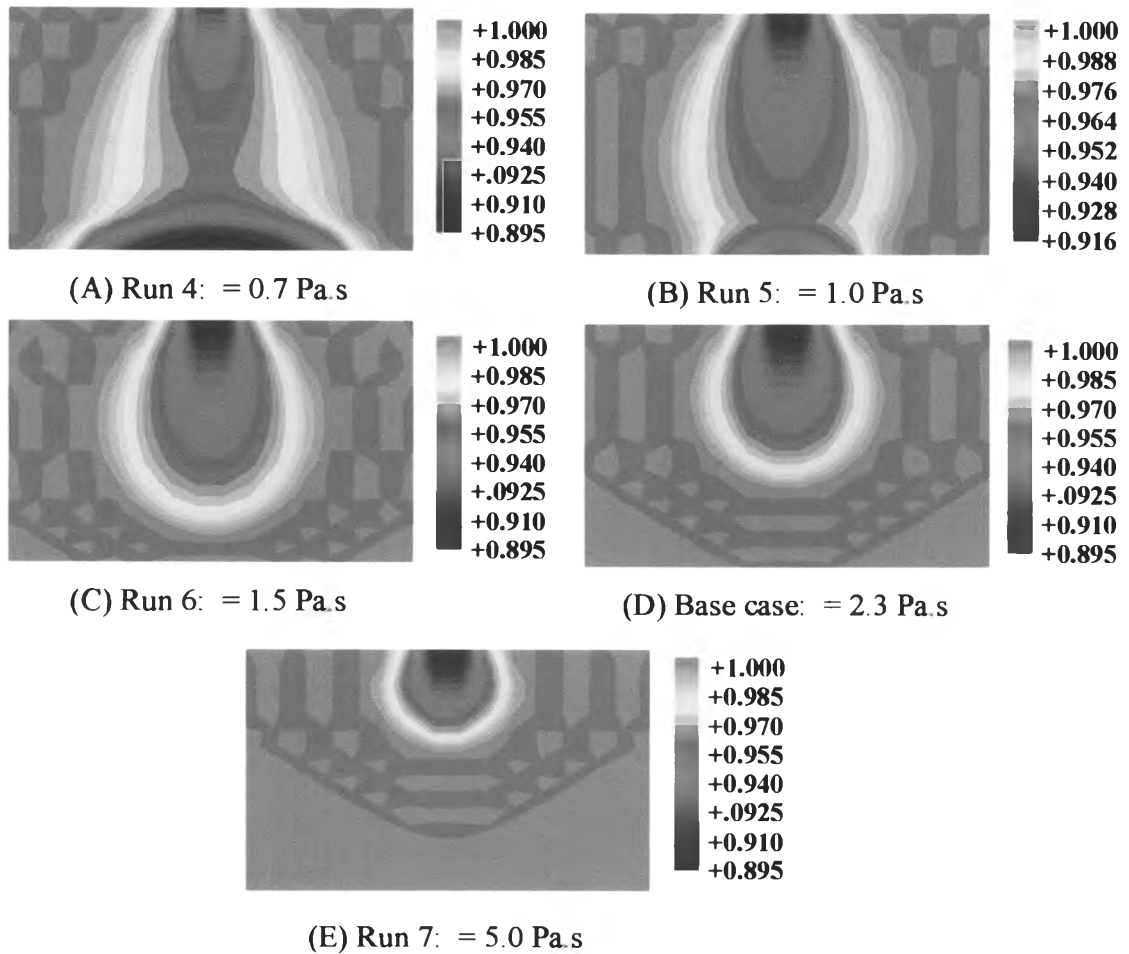


**Figure 4.4:** Water saturation contours showing the distribution of DNAPL at t of 50 seconds for various viscosities

(A,B,C) Runs 4, 5, 6 represents the case that viscosity of DNAPL is decreased.

(D) Base case simulation

(E) Run 7 represents the case that viscosity of DNAPL is increased.

The results for various DNAPL viscosities are shown in Figures 4.4.A-E. For the reduced viscosity case (RUNs 4-6), a much greater degree of plume spreading is evident for the specific time of  $t = 50$  seconds. Visual observations show that the lower viscosity DNAPL moves faster as shown in Figures 4.4.A-C. That is reasonable and can be explained by the hydraulic conductivity, which is inversely proportional to the viscosity, as shown in the equation:

$$K = \frac{k \times \rho g}{\mu}, \text{ so } K \propto \frac{1}{\mu}$$

Thus when the viscosity increases, DNAPL moves slower, as shown in Figure 4.4.E.

### 4.1.3 Effect of water flow in saturated porous media

This case is simulated to show movement patterns of DNAPL affected by water flow. When a DNAPL spills or leaks from an underground storage tank, it will move downward to the water table and then penetrate the water table. When the groundwater is flowing, the DNAPL cannot just move downward vertically to the bottom of the aquifer, but it will also move in the direction of groundwater flow.

To investigate the behavior of DNAPL when the groundwater is flowing, a contaminated site of 0.7 m wide and 0.5 m high is set up with the water table at the top boundary. The top and bottom boundaries are set as impermeable boundaries except for the DNAPL source (2.5 cm. wide) as shown in Figure 4.5. At the DNAPL source  $Q_N$  is set to  $5 \times 10^{-6} \text{ m}^3/\text{s}$  and  $Q_w$  is set to 0. The top and bottom boundaries are set as zero flow for water and DNAPL.

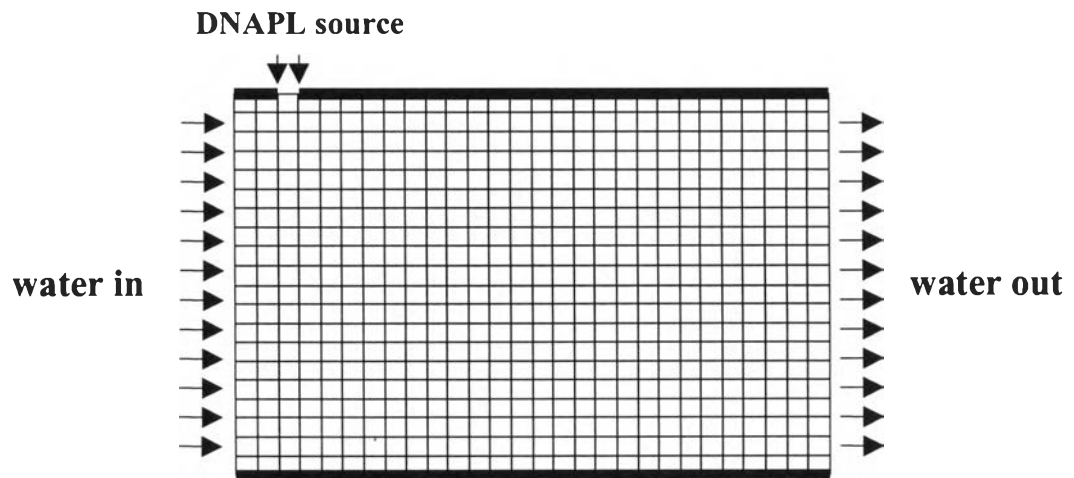


**Figure 4.5:** Solution domain for studying the effect of water flow on DNAPL transport

Water is allowed to come in from the left side and go out of the right side of the solution domain. The side boundaries of the solution domain are controlled by pressure of water. On the right side, the water pressure is hydrostatic. At the same depth, the pressure of water on the left side is 4.0 kPa greater than the right side.

The solution domain is divided using node spacing of 0.025 meter in the horizontal and vertical directions resulting in 20 x 28 elements. Material parameters are shown in Table 4.3.

Results of DNAPL distribution at different times are shown in Figure 4.6. The groundwater flow from left side to right side forces DNAPL to move down and right. After DNAPL reaches the bottom, it starts to move horizontally in the same direction as the groundwater flow.

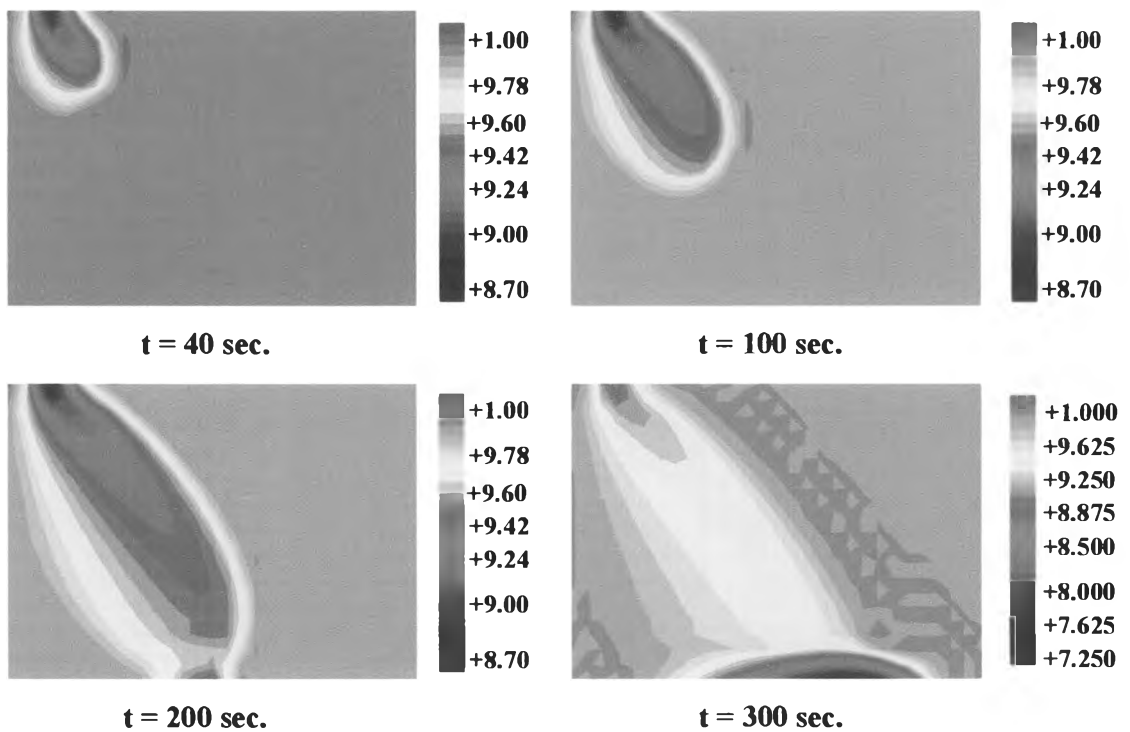


**Figure 4.6:** Water saturation contours at various times for studying the effect of water flow on DNAPL transport

**Table 4.3:** Material parameters for studying the effect of water flow in saturated porous media

Material parameters	Symbols	Values
Soil grain density	$\rho_s$	$2.7 \times 10^3 \text{ kg/m}^3$
Water density	$\rho_w$	$1.0 \times 10^3 \text{ kg/m}^3$
DNAPL density	$\rho_N$	$2.50 \times 10^3 \text{ kg/m}^3$
Bulk modulus of water	$K_w$	$0.43 \times 10^{10} \text{ kPa}$
Bulk modulus of DNAPL	$K_N$	$1.0 \times 10^6 \text{ kPa}$
Water viscosity	$\mu_w$	$1.0 \times 10^{-3} \text{ Pa.s}$
DNAPL viscosity	$\mu_N$	$5.0 \times 10^{-3} \text{ Pa.s}$
Intrinsic permeability	$K$	$5.0 \times 10^{-10} \text{ m}^2$
Irreversible water saturation of soil	$S_{irr}$	0.078
van Genuchten parameter	$\lambda$	$0.11 \text{ cm}^{-1}$
	$n$	1.84
Soil porosity	$n$	0.4
Initial water saturation	$S_{int}$	1.0

#### 4.1.4 LNAPL movement in confined saturated porous media

The modified U\_DYSAC2 computer code has been used to simulate a three-phase system: soil, water, and NAPL. In the previous cases, DNAPL movements were simulated. LNAPL movement is simulated here. U\_DYSAC2 cannot simulate a four-phase system such as a soil-water-air-NAPL system. Therefore in order to avoid LNAPL movement through the unsaturated zone, the simulation is done for a confined aquifer.

The simulation uses the same conditions as in Case 4.1.1 and also the same soil and fluid parameters as in Table 4.1, but the density of NAPL is changed to  $0.7 \times 10^3 \text{ kg/m}^3$ .

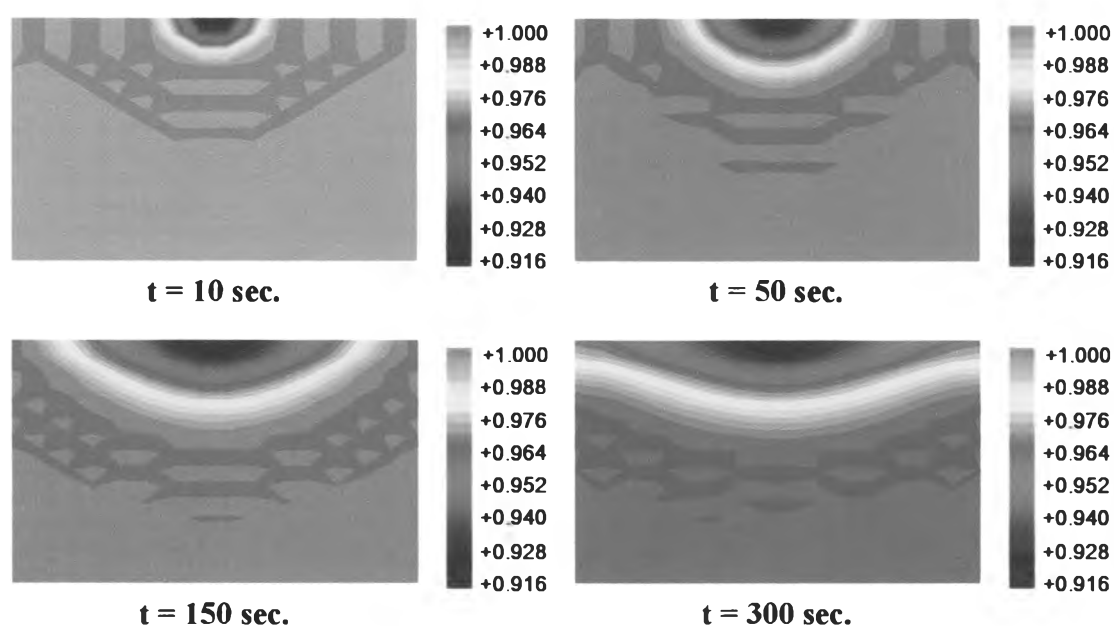


**Figure 4.7:** Water saturation contours showing the LNAPL movement in a confined aquifer

LNAPL movement patterns are shown in Figure 4.7 as the contours of water saturation. Figure 4.7 shows reasonable results. At a time of 10 seconds, LNAPL plume spreads in the same way as DNAPL. Because the NAPL head at the source, plume shape is semi-circular. Later LNAPL plume starts to spread horizontally.

Because LNAPL density is lower than water, the plume cannot move downward into the saturated media. After sometime, LNAPL starts to accumulate on top of the top layer. The LNAPL cannot move out of the box because of the impermeable layers on the top and lateral sides.

From sections 4.1.2-4.1.3, the results show that all parameters that have been studied affect the transport pattern of DNAPL. The results from varying NAPL viscosity and density show reasonable trends. The groundwater flow is also shown to affect the direction of the DNAPL plume. The results presented in Section 4.14 show that LNAPL movement in a confined aquifer can also be reasonably simulated using the modified U\_DYSAC2.

## 4.2 Comparison with experimental cases

This section presents comparisons of modified U\_DYSAC2 simulations and experimental results to validate the U\_DYSAC2 predictions.

### 4.2.1 Centrifuge study of low density high viscosity DNAPL in saturated porous media

This case study is based on an experiment performed by Pantazidou et al. (2000). Centrifuge experiments have been used to study NAPL transport patterns by elevating the gravity level to accelerate velocity of DNAPL movement. A smaller size model with a reduced head can also be used in the centrifuge. The test model is a box of glass beads as shown in Figure 4.8. Two perforated side partitions, covered with a fine mesh, were used to contain the porous medium and allow fluid to drain out of the box. These two side partitions also controlled the water table at the top of the medium.

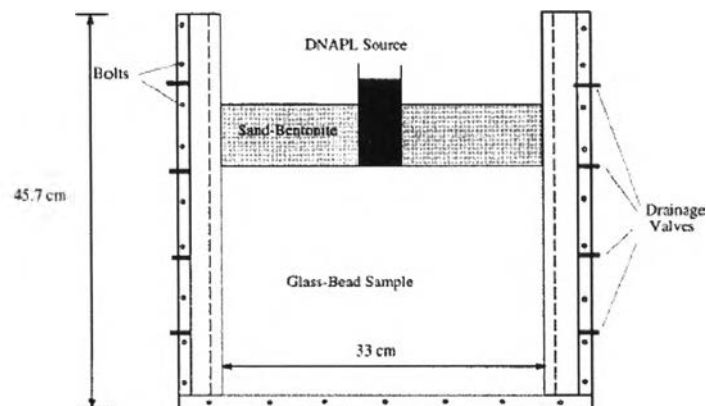


**Figure 4.8:** Front view of the centrifuge test model (Pantazidou et al. 2000)

The bottom of the set up is covered with a fine mesh that lets fluid drain out of the box. An impervious layer covers the top except at the location of the 7.5 cm-wide DNAPL source. The head pressure at the DNAPL source is 15.2 cm of DNAPL.

The DNAPL used in this model is Butyl Phthalate (BP). BP has a density of  $1.05 \times 10^3 \text{ kg/m}^3$  that is very close to that of water. BP's viscosity is 20.3 Pa.s, which is high when compared with water. The properties of BP are in the same range as coal tar and creosote. The glass bead medium is fully saturated when the simulation starts and has a porosity of 0.42 and a hydraulic conductivity of  $9 \times 10^{-3} \text{ cm/s}$ . The experiment is conducted by increasing the gravity force from 1g to 5g.

The experimental results are shown in Figure 4.9 as 2 dimensional DNAPL distributions in the soil-water system. At the beginning of the infiltration, the front velocity is at its highest, and subsequently it decreases monotonically to zero. The DNAPL front generally remains smooth, which shows stable displacement of water by the DNAPL.

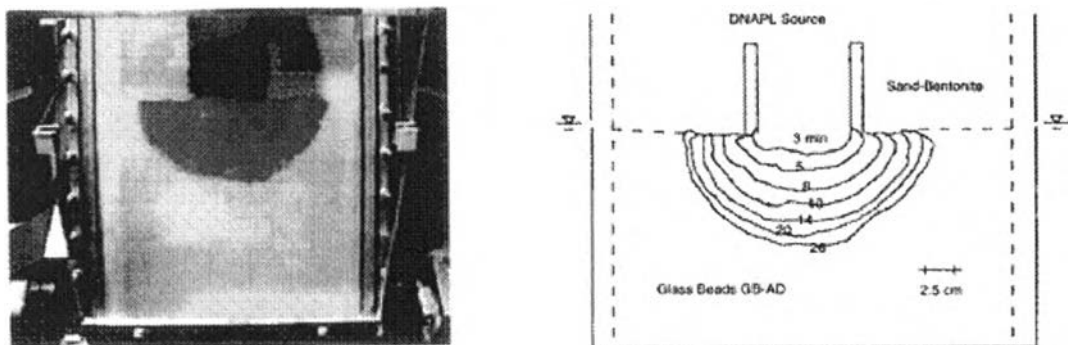


**Figure 4.9:** Experimental results for a low density, high viscosity DNAPL flow in a saturated porous medium (after Pantazidou et al. 2000)

To simulate this experiment, the solution domain cell is divided into 400 elements (16 cm-high x 33 cm-wide) as shown in Figure 4.10. Physical properties of soil, water and BP are obtained from the original experiment (Pantazidou et al. 2000). The boundary conditions are set as follows:

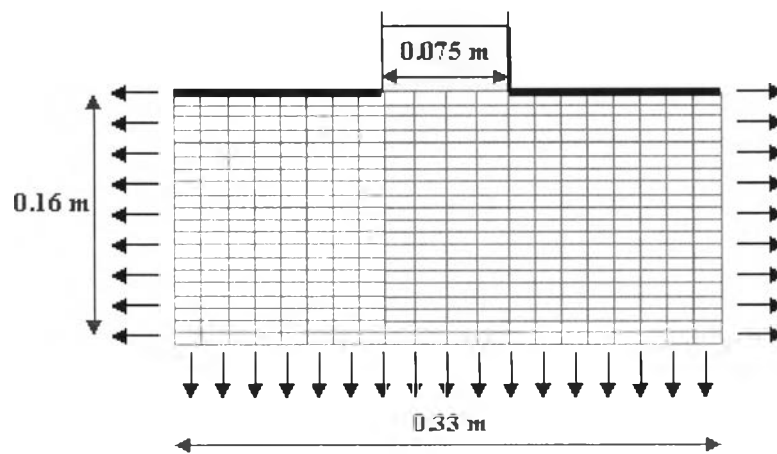
$$\begin{aligned} \text{BP source} & : Q_w = 0 \text{ cm}^3/\text{min}, P_N = 7.828 \text{ kPa}^* \\ \text{Top} & : Q_w = 0 \text{ cm}^3/\text{min}, Q_N = 0 \text{ cm}^3/\text{min} \end{aligned}$$

Side :  $P_w = P_N =$  increasing by depth from water table from 0 kPa to 7.848 kPa at bottom\*

Bottom :  $P_w = P_N = 7.848$  kPa\*

(\*) = pressure at 5g in experiment.

The simulation is run by increasing the gravity force from 0g to 5g. All of (\*) values will increase rapidly from 0 to those values (5g) in 1 minute to represent centrifuge conditions in the real experiment.

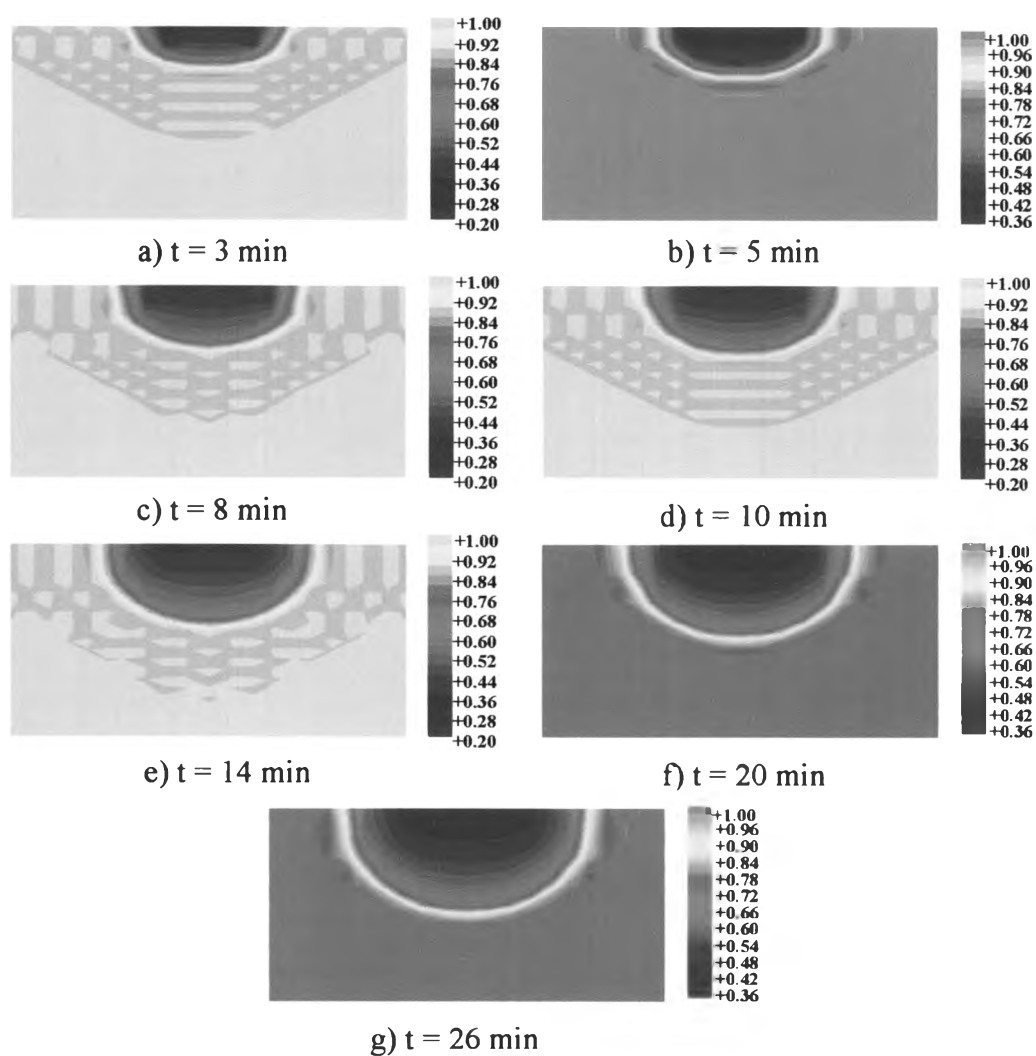


**Figure 4.10:** Finite element mesh for the centrifuge model

The data given by Pantazidou et al. (2000) are not sufficient to obtain the van Genuchten model parameters for glass beads and BP. Lenhard and Parker (1987) provided data to calculate van Genuchten parameters for p-cymene and various porous media. These parameters were scaled by the ratio of p-cymene interfacial tension to BP interfacial tension to obtain the necessary parameters for this simulation. Table 4.4 shows the estimated parameters.

**Table 4.4:** Scaling van Genuchten parameters for BP-water system.

p-cymene interfacial tension*	34.61 (dyn/cm)
BP interfacial tension*	27.0 (dyn/cm)
Parameters from Lenhard and Parker (1987) experiments (p-cymene and water in sandy soil)	$\alpha = 0.11 \text{ cm}^{-1}$ $n = 1.84$
Estimated parameter for simulation (BP and water in sandy soil)	$\alpha = 0.152 \text{ cm}^{-1}$ $n = 1.84$

**Figure 4.11:** Water saturation contours: showing distribution of BP versus time from 3 to 20 min.

The results from simulation are shown in Figure 4.11 and Figure 4.12. The simulation results compare reasonably well with experimental results. At the beginning of BP movement, the velocity is the highest. After that it decreases and approaches zero because the distance from the source negates the effect of DNAPL head. BP cannot move downward because its density is very close to that of water. The final shape of the plume is semi-circular. The experimental results show some differences from numerical results, such as; the movement of DNAPL plume for times less than 10 minutes is faster in the simulation than the experiment, and the shape of experimental results are as not smooth as in the simulation likely due to the heterogeneity of the glass bead medium.

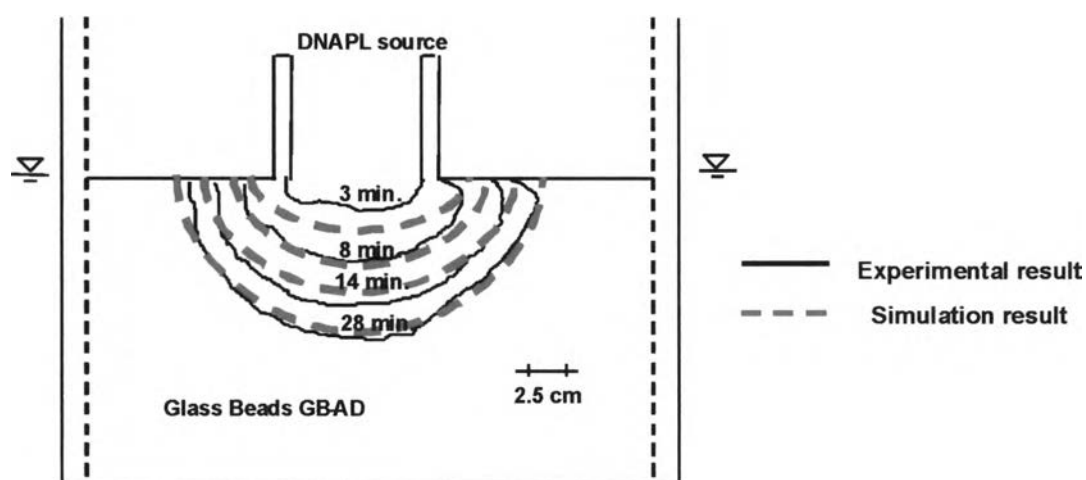


**Figure 4.12:** Comparison of predicted water saturation contours and visually observed DNAPL front at various times.

Additional numerical simulations showed that the extent of the plume is not very sensitive to different capillary pressure curves (Figure 4.13) as shown in Figure 4.14. These results confirm that the media dissimilarity with respect to the relationship of capillary pressure and water saturation curve does not have a significant effect on the predicted extent of a high viscosity and low density DNAPL.

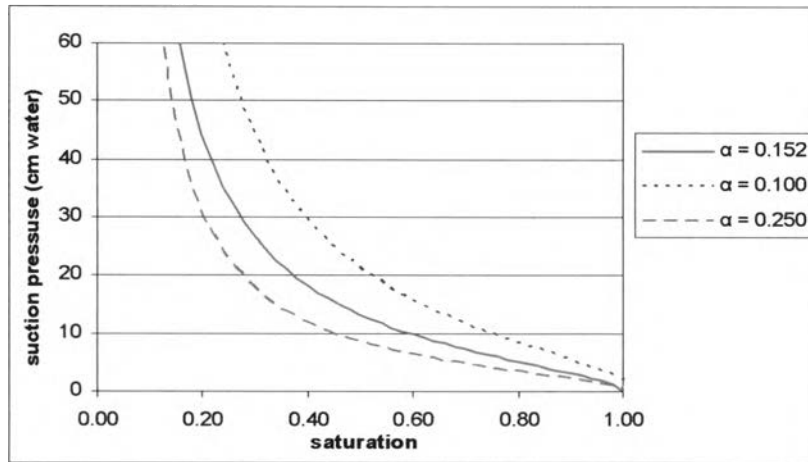


**Figure 4.13:** Capillary pressure-water saturation curves with different values of the  $\alpha$  parameter ( $n = 1.84$ )

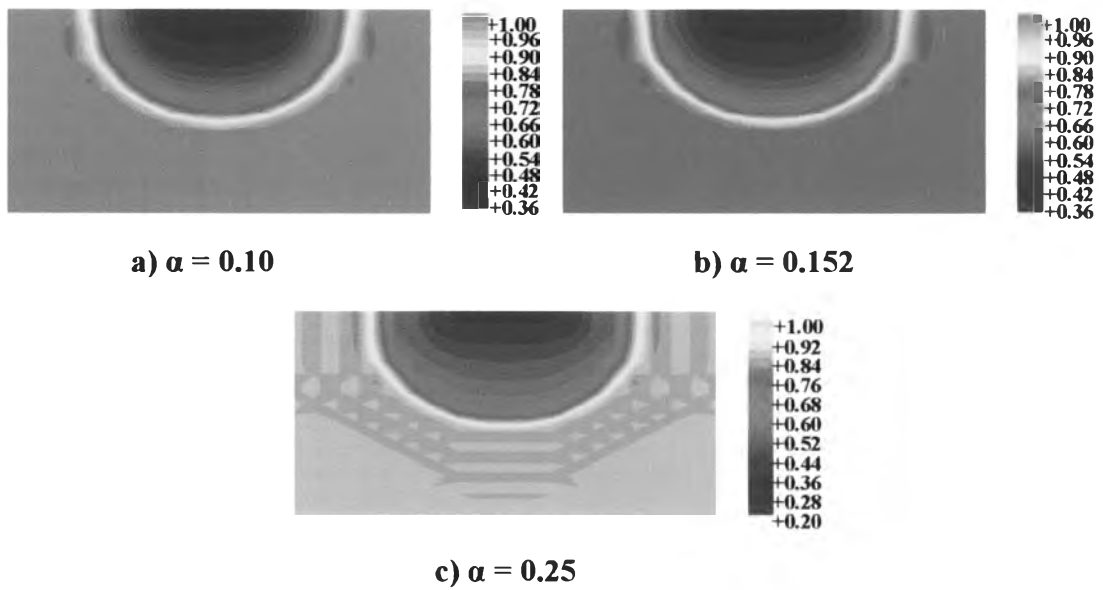


**Figure 4.14:** Water saturation contours: comparison between different capillary saturation curves.

#### 4.2.2 DNAPL transport in heterogeneous soil structure

This case is based on an experiment reported by Kueper and Frind (1991). The experiment is conducted to study DNAPL transport in heterogeneous media. Tetrachloroethylene (PCE) is used as the DNAPL phase. A 60-cm-high x 80-cm-wide x 0.6-cm-thick parallel-plate glass-lined cell is used. The cell was packed with four different silica sands. The configuration of the assembled sand is shown in Figure 4.15. Physical properties of each sand type are shown in Table 4.5.

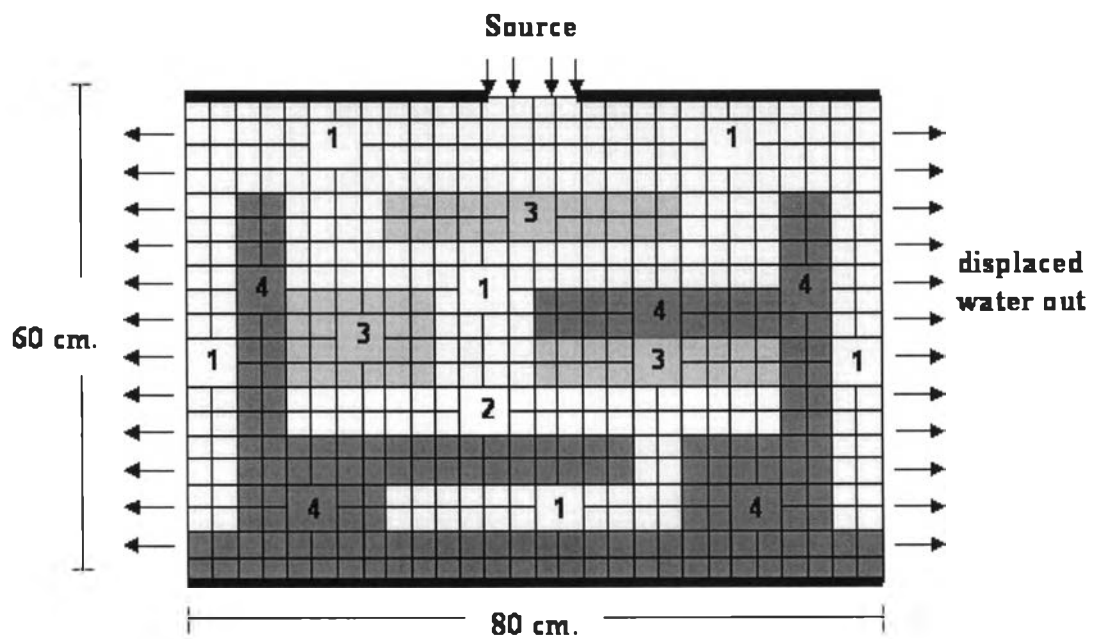


**Figure 4.15:** Configuration of packed sand in parallel-plate cell.

**Table 4.5:** Hydraulic properties of sand in parallel-plate lab experiment.

Sand	$S_{irr}$	$k$ ( $m^2$ )	Porosity
1)#16 silica	0.078	5.04 E-10	0.40
2)#25 ottawa	0.069	2.05 E-10	0.39
3)#50 ottawa	0.098	5.26 E-11	0.39
4)#70 silica	0.189	8.19 E-12	0.41

The bottom of the cell is sealed with an impermeable layer for both fluids. The top boundary is similarly sealed except the center 10 cm, which is opened for the source of PCE. Source pressure is controlled by head at 4.0 cm of PCE and maintained constant throughout the experiment. Two vertical sides are covered with wire screen to keep sand within the cell. The wire provides lateral outflow for water being displaced by PCE and the pressure is controlled by constant water pressure.

At the beginning of the experiment, PCE, which is colored by a nonvolatile dye, is released into the initially water-saturated cell. The observed distributions of fluid at each time are plotted into pictures as shown in Figure 4.16.

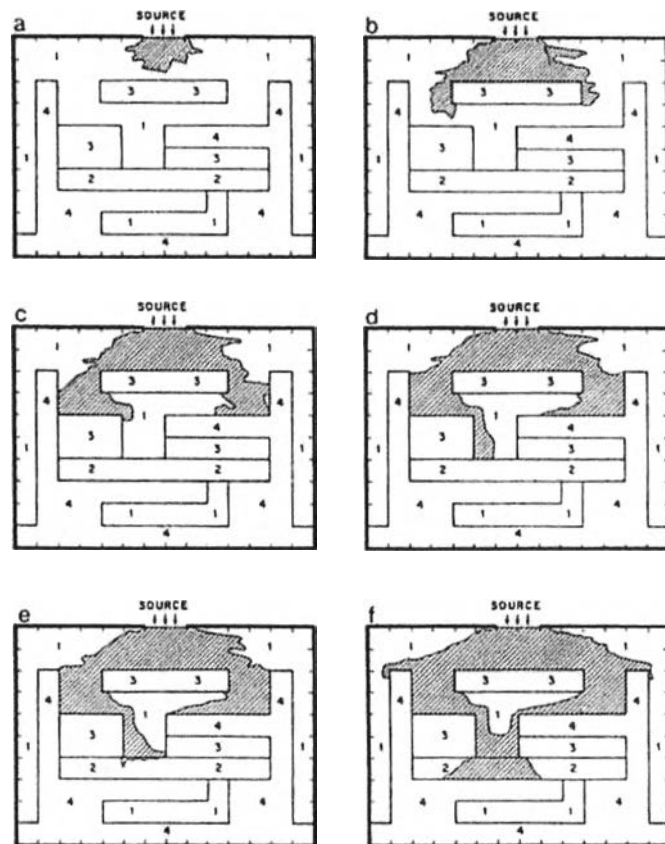


**Figure 4.16:** Observed distributions of PCE

(Kueper and Frind (1991)).

(a)  $t = 34$  sec.

(b)  $t = 126$  sec.

(c)  $t = 184$  sec.

(d)  $t = 220$  sec.

(e)  $t = 245$  sec.

(f)  $t = 313$  sec.

To simulate the experiment, the solution domain cell is divided into 480 elements (28 x 20). Input material parameters are shown in Table 4.7. Parameters given by Lenhard and Parker (1987) are used to estimate van Genuchten parameters for this case by assuming all four sand types as sandy soil media and scaling the parameters with the interfacial tension ratio of p-cymene to tetrachloroethylene. Table 4.6 shows the estimated parameters for each sand type. The boundary conditions for simulation are set as,

Source :	$P_w = 0 \text{ Pa}, P_N = 639.35 \text{ Pa}$
Top :	$Q_w = 0 \text{ Pa}, Q_N = 0 \text{ Pa}$
Bottom:	$Q_w = 0 \text{ Pa}, Q_N = 0 \text{ Pa}$
Side :	$P_w = \text{vary by height (0 to 4.905 Pa)}$

**Table 4.6** Scaling van Genuchten parameters for PCE-water system

p-cymene interfacial tension*	34.61 (dyn/cm)
Tetrachloroethylene interfacial tension*	47.48 (dyn/cm)
Parameters from Lenhard and Parker (1987) experiments (p-cymene and water in sandy soil)	$\alpha = 0.11 \text{ cm}^{-1}$ $n = 1.84$
Estimated parameters for simulation (tetrachloroethylene(PCE) and water in sandy soil)	$\alpha = 0.08 \text{ cm}^{-1}$ $n = 1.84$

\* = data reported by Demond and Lindner (1993)

Figure 4.17 shows the numerical results for times approximately equal to those in Figure 4.16. Because the experimental results are visual observations that do not show the concentration of DNAPL, the comparison between simulation and experiment cannot be made quantitatively. The dissimilarity between the simulated and observed results is the speed of the DNAPL plume. Some of the discrepancies are likely because the van Genuchten parameters were estimated and not measured.

However, when comparing transport patterns, the agreement between the two sets is quite reasonable. It shows that the modified U\_DYSAC2 code can be used to

explain the behavior of DNAPL when it penetrates through a heterogeneous soil structure.

**Table 4.7 :** Material parameters for simulation of DNAPL flow through heterogeneous soil structure.

Material parameters	Symbols	Values
Soil grain density*	$\rho_s$	$2.7 \times 10^3 \text{ kg/m}^3$
Water density	$\rho_w$	$1.0 \times 10^3 \text{ kg/m}^3$
DNAPL density	$\rho_N$	$1.63 \times 10^3 \text{ kg/m}^3$
Bulk modulus of water	$K_w$	$0.43 \times 10^{10} \text{ kPa}$
Bulk modulus of DNAPL*	$K_N$	$1.0 \times 10^6 \text{ kPa}$
Water viscosity	$\mu_w$	$1.0 \times 10^{-3} \text{ Pa.s}$
DNAPL viscosity	$\mu_N$	$0.9 \times 10^{-3} \text{ Pa.s}$
Initial water saturation	$S_{int}$	1.0

\* = assumed parameter

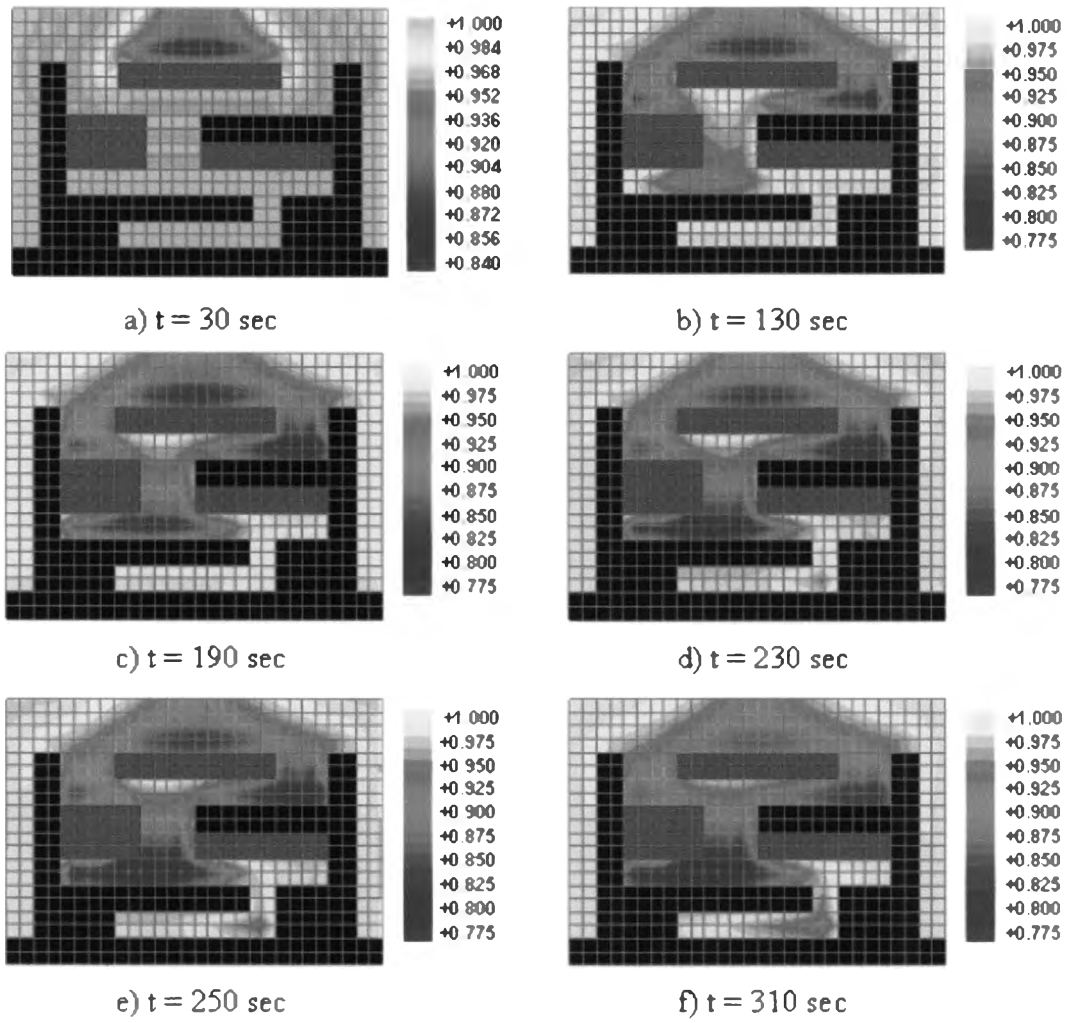


**Figure 4.17** : Simulation results of DNAPL flow through heterogeneous soil structure.